Science Journal of Chemistry
2023; 11(5): 189-196
http://www.sciencepublishinggroup.com/j/sjc
doi: 10.11648/j.sjc.20231105.12
ISSN: 2330-0981 (Print); ISSN: 2330-099X (Online)

Graphene-Like Biochar from Agricultural Waste for Cyanide Removal: Kinetic Study and Adsorption Isotherms

Djè Daniel Yannick[1], Yacouba Zoungranan[2, *], Kouassi Kouadio Dobi-Brice[1], Ekou Lynda[1], Ekou Tchirioua[1]

[1]Department of Chemistry, University NANGUI ABROGOUA, Abidjan, Côte d'Ivoire

[2]Department of Mathematics, Physics and Chemistry, University Peleforo GON COULIBALY, Korhogo, Côte d'Ivoire

Email address:

zoungranan@gmail.com (Yacouba Zoungranan), zoungranan@upgc.edu.ci (Yacouba Zoungranan)

[*]Corresponding author

To cite this article:

Djè Daniel Yannick, Yacouba Zoungranan, Kouassi Kouadio Dobi-Brice, Ekou Lynda, Ekou Tchirioua. Graphene-Like Biochar from Agricultural Waste for Cyanide Removal: Kinetic Study and Adsorption Isotherms. *Science Journal of Chemistry*. Vol. 11, No. 5, 2023, pp. 189-196. doi: 10.11648/j.sjc.20231105.12

Received: August 17, 2023; **Accepted**: September 7, 2023; **Published**: September 20, 2023

Abstract: Cyanide is well-known for its toxic nature and is frequently employed in the mining and chemical industries. The discharge of wastewater containing cyanide into the natural environment in various forms poses a serious threat to human health and the ecosystem. In fact, its presence can inhibit mitochondrial function in humans, leading to headaches, dizziness, irregular heartbeat, convulsions, fainting, and even death. As part of the study, an approach was developed for removing cyanide through adsorption on an adsorbent that contains graphene. The process of collecting and converting agricultural waste led to the obtention of this adsorbent. Oil palm shells were used to prepare graphene-like biochar (GpB). The obtained GpB was characterized by X-ray diffraction and its ash content, humidity, and zero charge point pH were determined. The adsorption efficiency was assessed using parameters such as initial concentration, adsorbent mass, and contact time. According to the study, 0.1 g of GpB in 50 ml of cyanide solution resulted in a 97.39% elimination after 60 minutes of equilibrium time. The study of adsorption kinetics demonstrated that GpB's cyanide removal process is chemisorption, which follows the pseudo-second order kinetic model. The Freundlich and Temkin isotherms better describe the adsorption of cyanide on GpB, confirming the presence of multilayers and an exothermic reaction.

Keywords: Adsorption, Cyanide, Oil Palm Shells, Graphene, Models

1. Introduction

The mining industry is seen as an engine of growth that can accelerate socio-economic development in producing countries. The industrial gold mining has grown considerably in Côte d'Ivoire over the last few decades. There has been an increase of over 5 tons in gold exports from 32.478 tons in 2019 to 38.523 tons in 2020 [1]. Unfortunately, as a result of illegal artisanal mining, known as gold panning, this positive dynamic has been disrupted. With the proliferation of gold panning across all regions of the country, health and environmental safety issues have emerged [2]. For ore processing and washing, gold-panning sites are generally located alongside watercourses. Wastewater from the various treatment processes is discharged into the environment without prior treatment, while many of the substances used in the treatment process are known to be pollutants, both for human and animal health. Indeed, chemicals such as mercury, cyanide, zinc and nitric acid are used in the chain of activity [3]. Intentional or accidental ingestion of cyanide can cause harm to humans, ranging from simple discomfort to serious pathologies leading to death [4-6]. Cyanide can be removed from contaminated environments using various chemical and physical treatment methods. Methods like electrocoagulation [7], bioremediation [8] and electro-oxidation [9] are already being utilized to eliminate cyanide from contaminated waters. The limitations of these methods stem from operating costs and the creation of hazardous by-products [10]. The adsorption method is an alternative to complex and costly removal methods, in which an adsorbate is attached to the

surface of an adsorbent [11-13]. The adsorption process involves the use of various adsorbents, such as activated carbon [14, 15] and zeolites [16]. These traditional adsorbents are rich in carbon; whose adsorption potential limits the internal sites [17]. The scientific community is increasingly interested in new synthetic adsorbents with extended structures, which is why this is happening. One of these new adsorbents is graphene, a monolayer of sp2-hybridized carbon. Graphene has a hydrophilic character and a high load density which can induce better adsorption capacity [18]. The primary source of graphene is either natural or synthetic graphite. High temperatures and high costs are necessary to obtain natural or synthetic graphite [19]. Furthermore, nanosheets derived from graphite are prone to self-aggregation in water and limit their ability to absorb pollutants [17]. Carbonaceous biomass is becoming increasingly used as a precursor material for obtaining graphene. In this study, palm shells (agricultural waste) are used as sources of carbon to produce biochar containing graphene (GpB). The conversion of biomass into a graphene-like material made up of stable nanosheets can solve the nanosheet self-aggregation problems mentioned earlier. The material developed and characterized will be used in tests to eliminate cyanide in an aqueous solution. The adsorption reaction will have its kinetic parameters and isotherms determined.

2. Material and Methods

2.1. Biomass

The oil palm (*Elaeis guineensis*) seeds of the dura x pisifera hybrid variety were used as source of carbon. They were collected as household waste in the city of Bonoua (5°16"N, 3°31"W), southeast of the economic capital Abidjan (Ivory Coast). The collected biomass was carried to the laboratory.

2.2. GpB Synthesis

The seeds of *Elaeis guineensis* were ground to separate the almonds from the shells. The resulting shells were thoroughly washed with distilled water and oven-dried (Memmert BM300, Schwabach, Germany) at 105°C for 48 h. The GpB synthesis was carried out in three (3) steps using the method of Xiao et al [17] with a few modifications specific to the study. The graphitisation-activation stage consisted of successively impregnating the dry shells of *Elaeis guineensis* with iron chloride ($FeCl_3$) and zinc chloride ($ZnCl_2$). In a 500 ml beaker, 100 grams of dry shells are placed. A $FeCl_3$ (3M) solution of 50 ml is added and it is heated to 150° C on a hot plate (Nanbei, NB-H-Pro, Zhengzhou, China) for 5 minutes. After 5 min of heating with continuous stirring, 50 ml of $ZnCl_2$ (3M) is added. The mixture is kept at 150°C and stirred continuously for 2 hours during the process. A substance that is black and viscous is formed. The mixture is cooled to room temperature (28°C), and then placed in an oven at 80°C for 24 hours. After the formation of a solid residue, graphitized biochar is formed. The biochar obtained is placed in a muffle furnace (Nabertherm Gmb, H., Bremen, Germany) at 900°C for 1 h with a gradient of 5°C/min. This last step ensures that the graphitized biochar turns into a graphene-type biochar after 1 hour of heating at 900°C. The solid residue obtained at the furnace outlet is cooled, crushed and then sieved on a sieve (Saulas, Paris, France) to retain particles with a diameter of less than 100 µm. To obtain the GpB, the sieve is washed to neutral pH and then oven-dried at 60°C for 24 hours. The control biochar CB was made from palm seeds without chlorides under similar temperature conditions.

2.3. Characterization

2.3.1. Moisture Content

In a ceramic crucible with mass m_0, GpB is added and the assembly's mass m_1 is taken at room temperature. The assembly is dried in the oven at 105°C for 24 hours and weighed after cooling to obtain a mass m_2. The process is repeated 3 times in the same temperature and pressure conditions. The moisture content (H) is determined according to the following formula:

$$H(\%) = \frac{m_1 - m_0}{m_2 - m_0} \times 100 \quad (1)$$

2.3.2. Ash Content

This method is used to identify the inorganic part of GpB. In a ceramic crucible with mass m_0, GpB is added and the whole mass m_1 is measured at room temperature. The whole is oven-dried at 105°C for 24 hours, then placed in a muffle furnace and calcined at 650°C for 1 hour. After cooling, the whole (crucible and ash) is weighed to give the mass m_2. Under the same temperature and pressure conditions, the process is repeated three times. The ash content (A) is determined according to the following formula:

$$A(\%) = \frac{m_1 - m_0}{m_2 - m_0} \times 100 \quad (2)$$

2.3.3. Zero Charge Point

The pH of zero charge point (pH_{PZC}) represents the pH at which the overall electrical charge of the GpB is zero, either through total absence of charge or through exact compensation of positive and negative charges. The importance of this parameter lies in the involvement of electrostatic forces in the adsorption process. At pH values above pH_{PZC}, the GpB surface will carry an overall negative charge. In a series of 7 x 250 mL beakers, each containing 50 mL NaCl solution (0.1 M), HCl (0.1M) or NaOH (0.1M) is added to adjust the initial pH values (pH_i) between 2 and 13. pH values are measured using a pH meter (Hanna HI 9813-5, Bucharest, Romania). Next, 1 g of GpB is placed in each beaker, and the mixture is kept under agitation for 48 h. After shaking and filtration, the final pH values (pH_f) of the solutions are determined. The plot $pH_f = f(pH_i)$ intersects the $pH_f = pH_i$ axis at the point of zero charge (pH_{PZC}).

2.3.4. GpB Density

An empty 100 mL test tube is weighed (M_0), filled to the gauge line with GpB and weighed again (M_1). GpB's density can be determined by:

$$d = \frac{M_1 - M_0}{100} \quad (3)$$

2.3.5. Identification of Structural Phases using XRD

The GBC-EMMA diffractometer (Braeside, Victoria, Australia) equipped with CuKα radiation (λ= 0.154 nm) was used to determine the structural phases of GpB using X-ray diffraction. Samples were analyzed in the 2θ range from 0.15 to 91 with a step size of 0.02.

2.4. Batch Study

2.4.1. Methodology

A stock of potassium cyanide stock solution at C_0 = 50 mg/L was carefully prepared for all tests. The stock solution was diluted to obtain the various C_i concentrations. For each experiment, a mass m = 0.1 g of GpB is placed in a 250 ml beaker containing V_i = 50 ml of potassium cyanide at the C_i concentration. In order to prevent the cyanide from evaporating, the beaker is covered with film (Parafim, PM-996, USA). The mixture (cyanide-GpB) is stirred at 300 rpm for a given time using a vibrating shaker (Heidolph Vibramax 100, Germany). After stirring, the mixture is filtered to obtain a final volume V_f. The pyridine-pyrazalone method is used to analyze residual cyanide using HACH powder cyanide reagents in hermetically sealed bags (100 tests). A volume of 10 ml of the filtrate is taken to undergo the complexion stages with cyanide reagents 3, 4 and 5 (cyaniver 3, cyaniver 4 and cyaniver 5).

The first step is to add one sachet of cyaniver 3 to 10 ml of filtrate taken from a test tube. The tube is covered with parafilm and shaken vigorously by hand for 30 seconds before being left to stand for another 30 seconds. Then, the content of cyaniver 4 is adding and shakes it for 10 seconds. Finally, the contents of the cyaniver 5 sachet are added to the mixture, shaken again, and left to stand for another 30 minutes. During this time a blue coloration appears, revealing the complexation of the cyanide. Distilled water is used as a control sample to carry out the same procedure. Using a UV-visible photospectrometer (WFJ-752, China), optical density was read at 612 nm. The C_i (initial) and C_f (final) concentrations are determined using the calibration curve performed with a potassium cyanide solution in bi-distilled water.

$$q = \frac{C_i V_i - C_f V_f}{m} \quad (4)$$

2.4.2. Effects of Some Physicochemical Parameters

To study the effect of GpB contact time in solution, eight (8) beakers were placed with 0.1 g of GpB. Each beaker contains 50 ml of cyanide solution at C_i = 1 mg/L. The stirring times for each beaker were set at 5, 10, 15, 30, 45, 60, 90, and 120 minutes.

The influence of the initial concentration of the cyanide solution on absorption efficiency was evaluated with C_i concentrations of 1, 2, 4, 6, 8 and 10 mg/L. The stirring time for these tests was set to one hour, with stirring at 300 rpm.

The effect of the GpB mass in the solution was assessed by placing 0.1, 0.2, 0.3, 0.4 and 0.5 g GpB in a potassium cyanide solution (1 mg/L), for 1 hour at 300 rpm.

2.4.3. Adsorption Kinetics

To better understand all the steps involved in controlling the rate of GpB adsorption (mass transport processes and chemical reaction), three kinetic models were applied to the experimental data from the contact time study. These kinetic models included equations pseudo-first order, pseudo-second order, Elovich and intraparticle diffusion.

In linear form, the pseudo-first-order model or Lagergren equation (1898) [20] is represented by:

$$\log(q_e - q_t) = \log(q_e) - \frac{k_1}{2.303} = f(t) \quad (5)$$

Where q_e and q_t (mg/g) are, respectively, the adsorption capacity at equilibrium and at time t (min). k_1 (min^{-1}) is the reaction rate constant.

The pseudo-second order model [21] is represented in its linear form by the following expression:

$$\frac{t}{q_t} = \frac{1}{k_2 q_e^2} + \frac{1}{q_e} t = f(t) \quad (6)$$

Where q_e and q_t (mg/g) are, respectively, the adsorption capacity at equilibrium and at time t (min). k_2 (min^{-1}) is the reaction rate constant.

The chemical interaction between the adsorbate and the adsorbent surface is reflected in Elovich's model [22]. The model is presented in a linear form by:

$$q = \frac{1}{\beta}\ln(\alpha\beta) + \frac{1}{\beta}\ln(t) = f(t) \quad (7)$$

With α the initial adsorption rate (mg/g.min) and β the desorption constant related to surface area and reaction activation energy.

Diffusion is one of the steps involved in adsorption kinetics. The equation [23] is used to describe the intra-particle diffusion model.

$$q_t = k_d t^{0.5} + C = f(t^{0.5}) \quad (8)$$

k_d ($mg/g.min^{0.5}$) is a diffusion constant and C is the boundary layer thickness.

2.4.4. Adsorption Isotherms

Adsorption isotherms are employed to characterize the properties of adsorption surfaces and predict the adsorption reaction's nature. The present study tested three adsorption isotherms models that relate to adsorption equilibrium. These

are the Langmuir, Freundlich and Temkin isotherms.

The Langmuir model is based on the assumption that the adsorbent surface has monolayer adsorption, with a finite number of adsorption sites and uniform adsorption energies [24].

The Langmuir equation is given linearily by:

$$\frac{C_e}{q_e}=\frac{1}{q_m K_L}+\frac{1}{q_m}C_e=f(C_e) \quad (9)$$

The concentration of the cyanide solution is C_e (mg/L) and the amount of cyanide adsorbed at equilibrium is q_e (mg/g). K_L is the Langmuir constant and q_m the maximum adsorbed cyanide capacity. The Langmuir separation factor is utilized to determine the adsorbent's affinity for the adsorbent. It is given by the relation:

$$R_L=\frac{1}{1+K_L C_0} \quad (10)$$

When $R_L > 1$ adsorption is unfavorable, linear for $R_L = 1$, favorable when $0 < R_L < 1$ and irreversible if $R_L = 0$.

In a multilayer approach, the Freundlich isotherm describes a nonlinear adsorption process on a heterogeneous surface.

The Freundlich isotherm's linear form is as follows:

$$\log(q_e)=\log(K_F)+\frac{1}{n}\log(C_e)=f(C_e) \quad (11)$$

K_F (L/mg) is the adsorption capacity and 1/n (L/g) is the adsorption intensity, indicating the relative energy distribution and heterogeneity of adsorbed sites.

According to the Temkin isotherm, adsorption energy decreases with surface coverage, thus assuming linear adsorption energy [25, 26].

The linear form is

$$q_e=\frac{RT}{b_T}\ln(K_T)+\frac{RT}{b_T}\ln(C_e)=f(\ln(C_e)) \quad (12)$$

Where K_T is the Temkin coefficient linked to the nature of the adsorbent and the adsorbent and b_T the coefficient linked to the average adsorption energy.

3. Results and Discussion

3.1. GpB Characteristics

The synthesized GpB has a moisture content of 9.51 ± 0.10%, an ash content of 11.74 ± 0.12% and an apparent density of 0.76 ± 0.013 g/cm^3. GpB is a material that is low-moisture and has a ash content of less than 15%, which suggests that it is rich in mineral matter. This high ash content could be explained by metal enrichment during the graphitization-activation process by the metal chlorides. The attractiveness of Van Der Waals forces could be enhanced by this. The pHpzc (Figure 1) determination resulted in a value of 7.3, which indicates a positive GpB's surface at low pH values.

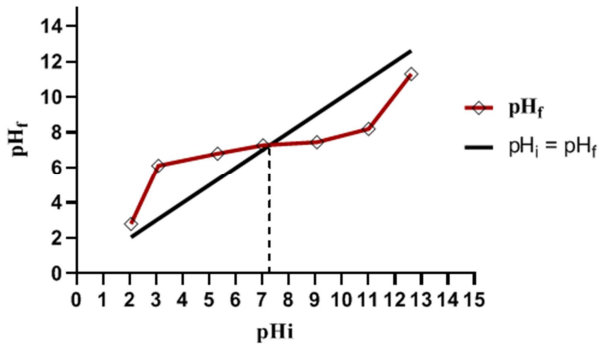

Figure 1. *Determination of pH at zero charge.*

The determination of the structural phases of CB (control biochar) and BGp by X-ray diffraction is shown in figure 2. The amorphous carbon structure is characterized by broad bands at high intensities in the CB difractogram. In the case of the difractogram GpB, there is an intense peak (at 26.03°) characteristic of the graphitic carbon. As we move from CB to GpB, peaks become more acute and intense, reflecting the transition to more organised structural phases. The finer and more intense reflection peaks of GpB indicate a higher degree of graphitisation, confirming a shift towards a graphene-like structure [27].

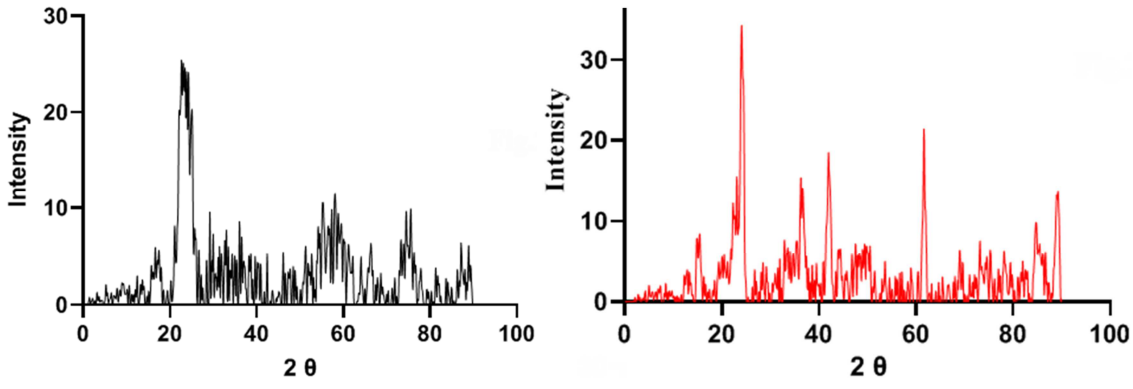

a b

Figure 2. *Diffractograms: a) control biochar CB; b) graphene-like biochar GpB.*

3.2. Influence of Some Physico-Chemical Parameters

Figure 3 illustrates the effects of certain physio-chemical parameters on cyanide adsorption on GpB.

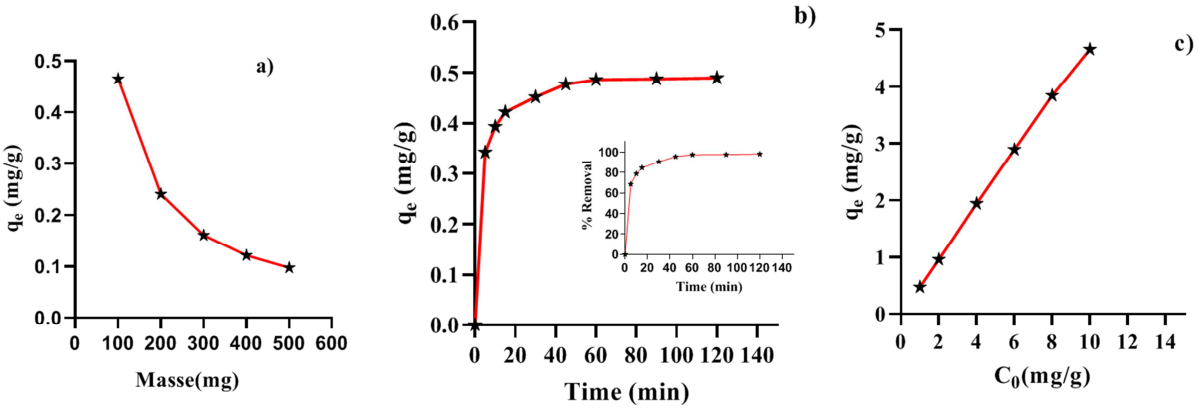

Figure 3. *Evolution of the quantity of cyanide adsorbed on GpB as a function of mass (a), time (b) and initial concentration (c).*

The amount of cyanide adsorbed increases as the mass of GpB is increased, as shown in figure 3-a). As the mass of GpB increases at constant volume, the amount of cyanide adsorbed decreases from 0.47 mg/g to 0.09 mg/g. As the volume of GpB in solution increases, there are more adsorption sites available for a given amount of cyanide in solution. The increase in GpB mass also induces the formation of GpB aggregates, which may reduce the number of adsorption sites available, thus limiting the removal rate. The result is similar to that of Sudipta Goswami et al. who showed an increase in adsorption efficiency with a simultaneous increase in adsorbent dosage [28].

Figure 3-b) shows the effect of the contact time of GpB with the cyanide solution. The uptake of cyanide on GpB is initially very fast, reaching chemical equilibrium after 60 min with an elimination rate of 97.39%. This removal rate is higher than that reported by Aliprandini [29] who achieved a removal rate of 81% of mercury cyanide using 0.1 g of activated carbon. This rapid initial adsorption means that active sites are available and are progressively saturated to reach adsorption equilibrium. The equilibrium can be reached by the stirring time, which is related to the experimental contact time. In fact, the longer the stirring time, the greater the driving force and the lower the resistance to mass transfer [30].

Figure 3-c) illustrates the effect of the initial cyanide concentration on the GpB adsorption capacity. As the initial concentration increases, the amount of cyanide adsorbed increases. The increase in the amount adsorbed is related to the increase in the driving force resulting from the concentration gradient. The resistance to mass transfer between the aqueous (cyanide) and solid (GpB) phases is reduced by this driving force [30].

3.3. Kinetic Models and Adsorption Isotherms

3.3.1. Kinetic Models

The contact time effect study's experimental results were utilized in intraparticle, pseudo-first-order, pseudo-second-order, and Elovich diffusion models. These outcomes are presented in Figure 4. Tables 1 and 2 present the parameters derived from these different model.

Table 1. *Parameters of adsorption kinetic models.*

q_{exp}	Pseudo-first-order			pseudo-second-order			Elovich		
	k_1	q_e	R^2	k_2	q_e	R^2	α	β	R^2
0.49	0.02	0.38	0.85	0.7	0.5	0.99	19.29	21.19	0.94

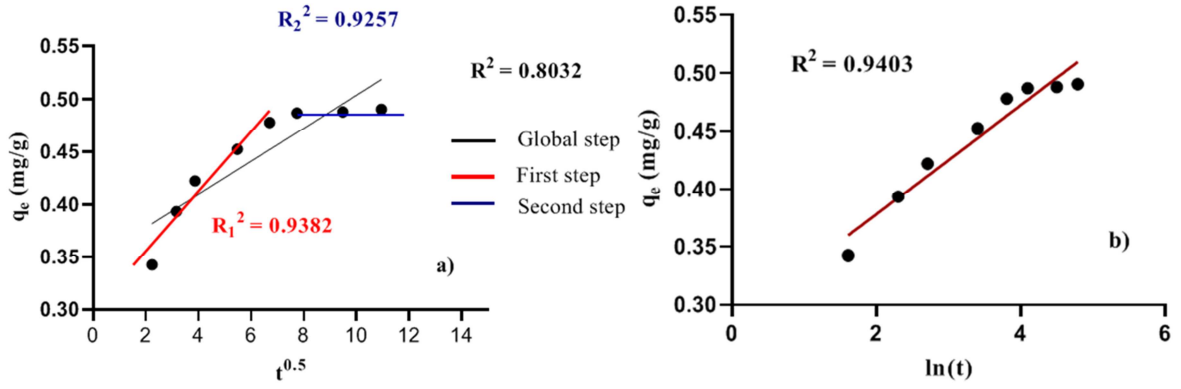

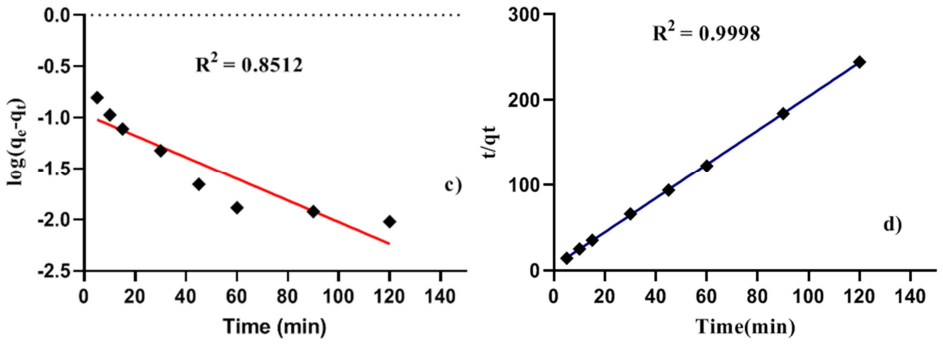

Figure 4. *a) Pseudo-first-order, b) pseudo-second-order and c) Elovich model and d) intraparticle.*

Table 2. *Intraparticle diffusion model parameters.*

Globale step			First step			Second step		
k_d	C	R^2	k_{d1}	C_1	R_1^2	k_{d2}	C_2	R_2^2
0.0157	0.3469	0.80	0.289	0.29	0.96	0.0011	0.4784	0.92

Figure 4-a) shows the result of the intraparticle diffusion phenomenon, making it possible to assess if the external diffusion stage is decisive for the overall reaction [31]. The overall reaction shows a linear regression that does not pass through the origin. This means that intraparticle diffusion does not control alone the velocity. Moreover, the value of k_d = 0.0157 mg/g.min$^{0.5}$ shows that the diffusion process is slow overall. Two stages are involved in the diffusion of intraparticles. The first is fast, with a diffusion coefficient k_{d1} = 0.2890 mg/g.min$^{0.5}$, reflecting the diffusion in the BPG macropores. The rate-limiting step in overall diffusion is the second, slow step (k_{d2} = 0.0011 mg/g.min$^{0.5}$). This is a slow step and reflects the diffusion into the micropores. Results from Elovich's model (Figure 4-b) show a good correlation with the experimental results. This suggests that chemisorption plays a decisive role in the adsorption of cyanide onto GpB. This chemisorption mechanism is corroborated by the results of the pseudo-second-order model test (Figure 4-c). For this model, the theoretical amount of cyanide adsorbed (q_{eth} = 0.5 mg/g) is very close to the value found experimentally (q_{exp} = 0.49 mg/g). A similar result on the tendency for cyanide chemisorption was observed by Behnamfard and Mehdi [32]. The cyanide adsorption process on GpB does not follow the pseudo-second-order model (Figure 4-d), thus ruling out the significant contribution of Van der Waals forces in cyanide adsorption on GpB.

3.3.2. Adsorption Isotherms

Figure 5 shows the results of the adsorption isotherms used to study the interaction forces between cyanide and GpB, with a view to predicting the nature of the adsorption reaction and understanding the stacking mode of the adsorbed layers. The various parameters of these models are given in Table 3.

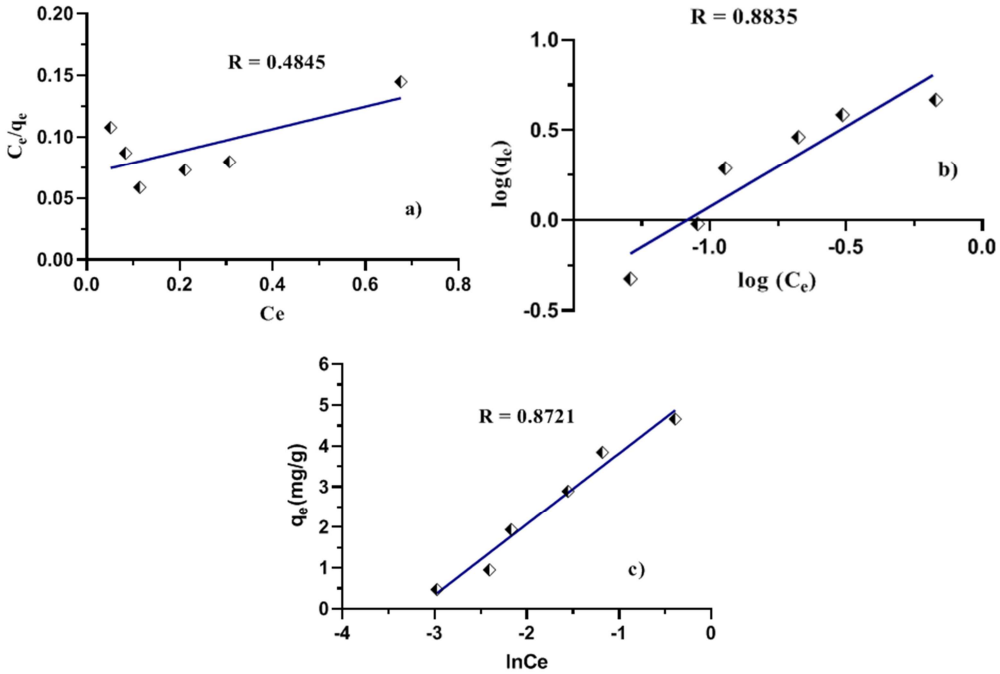

Figure 5. *Adsorption isotherm models tested: a) Langmuir; b) Freundlich; c) Temkin.*

Table 3. *Parameters of various adsorption isotherms tested.*

Parameters	Langmuir			Freundlich			Temkin		
	R^2	q_{max}	R_L	R^2	n	K_F	R^2	K_T	b_T (J/mol)
	0.48	11.38	0.14	0.88	1.11	9.25	0.97	24.38	1423.545

Figure 5-a shows that the experimental results do not follow the Langmuir model. This means that the adsorption surface is not homogeneous and uniform, and that there is a strong interaction between the adsorbed cyanide layers. However, the R_L value = 0.14 allows us to conclude that cyanide adsorption on GpB is favorable. The coefficient of determination R^2 = 88 and the value of the heterogeneity factor n= 1.11 > 1 in the Freundlich model test (Figure 5-b), show that cyanide adsorption is favorable and follows an L-type isotherm [33]. This result also suggests multilayer chemisorption [34, 35] on a heterogeneous surface. The Temkin model test (Figure 5-c) shows a good correlation with experimental values. The strong positive value of the constant b_T = 1423.546 J/mol shows that the adsorption reaction of cyanide on GpB is exothermic. [36, 37].

4. Conclusion

Oil palm shells (agricultural and household waste) were converted into graphene biochar (GpB) through graphitization and activation processes. XRD characterization of the material revealed a modification of the crystalline structure of the control biochar. The material also has a low moisture content and medium density, with a zero charge surface area of pH_{pzc} = 7.3. The resulting material was used for cyanide removal in a synthetic aqueous solution. Adsorption tests showed favorable adsorption according to the pseudo-second-order kinetic model. Chemisorption was confirmed by studying the adsorption isotherms. The adsorption isotherm is of type L and follows the Freundlich model. A correlation with the Temkin model was also found, confirming chemisorption and revealing the exothermic nature of the cyanide adsorption reaction on the GpB material. The study demonstrates that the biomass of oil palm shells can be converted into a graphene-like material for the removal of hazardous pollutants such as cyanide used in gold mining.

Acknowledgments

The authors would like to thank the Department of Chemistry of the University Nangui Abrogoua (RCI) and specifically the Laboratory of Thermodynamics and Environmental Physicochemistry, for the facilities made available to them to conduct this research work.

References

[1] Enerteam. (2020). “Initiative pour la Transparence dans les Industries Extractives de la Côte d’Ivoire. *Rapport-ITIE-CI-2020.*

[2] Goh Denis. (2016). L'exploitation Artisanale De L'or En Côte D’Ivoire: La Persistance D'une Activite Illegale. *European Scientific Journal.* vol 12. no 3. p 18 doi: 10.19044/esj.2016.v12n3p18.

[3] Virender Kumar, Vijay Kumar & T. Bhalla. (2013). In vitro cyanide degradation by Serretia marcescens RL2b. International *Journal on Environmental Sciences* vol 3 no 6., p 1969-1979. doi: 10.6088/ijes.2013030600019.

[4] P. Compagnon, D. Zabet, G. Drevin, B. Lelièvre, M. Briet & C. Abbara. (2020). Suicide au cyanure: à propos d’un cas. *Toxicologie Analytique et Clinique.* vol 32 no 4 p S41. doi.org/10.1016/j.toxac.2020.09.005

[5] B. Desharnais, G. Huppé, M. Lamarche, P. Mireault, & C. D. Skinner. (2012). Cyanide quantification in post-mortem biological matrices by headspace GC-MS. *Forensic Science International.* vol 222, no 1–3 10 pp 346-351. doi: 10.1016/j.forsciint.2012.06.017.

[6] Manila & P. Devi. (2021). Hydrogen cyanide: Risk assessment, environmental, and health hazard. *Hazardous Gases*. vol 15 p 183-195. doi: 10.1016/B978-0-323-89857-7.00010-4.

[7] M. K. Chegeni, A. Shahedi, A. K. Darban, A. Jamshidi-Zanjani, & M. Homaee. (2021) Simultaneous removal of lead and cyanide from the synthetic solution and effluents of gold processing plants using electrochemical method. *Journal of Water Process Engineering*. vol. 43, p. 102284. doi: 10.1016/j.jwpe.2021.102284.

[8] C. R. Lovasoa, K. Hela, A. A. Harinaivo, & Y. Hamma. (2017). Bioremediation of soil and water polluted by cyanide: A review. *African Journal of Environmental Science and Technology.* vol. 11 no. 6, pp. 272-291. doi: 10.5897/AJEST2016.2264.

[9] H. Wang, C. Gao, X. Li, CY. Liu, T. Yu, Y. Li, L. Liu & H. Wang. (2022). Electroreduction recovery of gold, platinum and palladium and electrooxidation removal of cyanide using a bioelectrochemical system. *Bioresource Technology Reports*. vol. 18, p. 101007. doi: 10.1016/j.biteb.2022.101007.

[10] M. M. Botz, T. I. Mudder, & A. U. Akcil. (2016). Cyanide Treatment: Physical, Chemical, and Biological Processes. *Gold Ore Processing*. pp. 619-645. doi: 10.1016/B978-0-444-63658-4.00035-9.

[11] Ju Lin, Tiezhu, Su, Jiawen, Chen, Tianwei, Xue, Shuliang Yang, Peiwen Guo, Hongying Lin, Hongtao Wang, Yanzhen Hong, Yuzhong Su, Li Peng & Jun Li. (2021). Efficient adsorption removal of anionic dyes by an imidazolium-based mesoporous poly (ionic liquid) including the continuous column adsorption-desorption process. *Chemosphere*. vol. 272, p. 129640doi: 10.1016/j.chemosphere.2021.129640.

[12] A. Leudjo Taka, M. J. Klink, X. Yangkou Mbianda, & E. B. Naidoo. (2020). Chitosan nanocomposites for water treatment by fixed-bed continuous flow column adsorption: A review. *Carbohydrate Polymers*. vol. 255 p. 117398. doi: 10.1016/j.carbpol.2020.117398.

[13] L. Das, S. Sengupta, P. Das, A. Bhowal & C. Bhattacharjee (2021). Experimental and Numerical modeling on dye adsorption using pyrolyzed mesoporous biochar in Batch and fixed-bed column reactor: Isotherm, Thermodynamics, Mass transfer, Kinetic analysis. *Surfaces and Interfaces*. vol. 23, p. 100985. doi: 10.1016/j.surfin.2021.100985.

[14] J. Xia, R. Marthi, J. Twinney, & A. Ghahreman. (2022). A review on adsorption mechanism of gold cyanide complex onto activation carbon. *Journal of Industrial and Engineering Chemistry*. vol. 111, pp. 35–42. doi: 10.1016/j.jiec.2022.04.014.

[15] G. G. Stavropoulos, G. S. Skodras & K. G. Papadimitriou. (2015). Effect of solution chemistry on cyanide adsorption in activated carbon. Applied Thermal Engineering. vol. 74, pp. 182–185. doi: 10.1016/j.applthermaleng.2013.09.060.

[16] I. Maulana & F. Takahashi. (2017). Cyanide removal study by raw and iron-modified synthetic zeolites in batch adsorption experiments. *Journal of Water Process Engineering*. vol. 22, no. September 2017, pp. 80–86. doi: 10.1016/j.jwpe.2018.01.013.

[17] X. Xiao, B. Chen, L. Zhu, & J. L. Schnoor. (2017). Sugar Cane-Converted Graphene-like Material for the Superhigh Adsorption of Organic Pollutants from Water via Coassembly Mechanisms. *Environmental Science and Technology*. vol. 51, no. 21, pp. 12644–12652. doi: 10.1021/acs.est.7b03639.

[18] P. Banerjee, S. Sau, P. Das, & A. Mukhopadhayay. (2015). Optimization and modelling of synthetic azo dye wastewater treatment using Graphene oxide nanoplatelets: Characterization toxicity evaluation and optimization using Artificial Neural Network. *Ecotoxicology and Environmental Safety*. vol. 119, pp. 47–57. doi: 10.1016/j.ecoenv.2015.04.022.

[19] U. Sierra, P. Álvarez, C. Blanco, M. Granda, R. Santamaría & R. Menéndez. (2016). Cokes of different origin as precursors of graphene oxide. *Fuel*. vol. 166, pp. 400–403. doi: 10.1016/j.fuel.2015.10.112.

[20] S. LAGERGREN. (1899). Zur theorie der sogenannten adsorption gelöster stoffe. *Kungliga Svenska Vetenskapsakademiens*. vol. 2, no. 4, pp. 1–39. doi: 10.1007/BF01501332.

[21] Y. S Ho & G. Mc Kay. (1999). Pseudo second order model for sorption processes. *Process Biochemistry*. vol. 34 no. 5, pp. 451-459. doi: 10.1016/S0032-9592(98)00112-5.

[22] M. J. D. Low. (1960). Kinetics of Chemisorption of Gases on Solids. *Chemical Reviews*. pp. 267–312. doi: 10.1021/cr60205a003.

[23] T. R. Sahoo & B. Prelot. (2020). Adsorption processes for the removal of contaminants from wastewater. *Nanomaterials for the Detection and Removal of Wastewater Pollutants*. pp. 161–222. doi: 10.1016/B978-0-12-818489-9.00007-4.

[24] A. Günay, E. Arslankaya & I. Tosun. (2007). Lead removal from aqueous solution by natural and pretreated clinoptilolite: Adsorption equilibrium and kinetics. *Journal of Hazardous Materials*. vol. 146, no. 1–2, pp. 362–371. doi: 10.1016/J.JHAZMAT.2006.12.034.

[25] C. Aharoni & M. Ungarish, (1977). Kinetics of activated chemisorption. Part 2. —Theoretical models. Journal of the Chemical Society, Faraday Transactions 1. *Physical Chemistry in Condensed Phases*. vol. 73, p. 456. doi: 10.1039/f19777300456.

[26] M. Vadi, A. O. Mansoorabad, M. Mohammadi & N. Rostami. (2013). Investigation of Langmuir, Freundlich and Temkin Adsorption Isotherm of Tramadol by Multi-Wall Carbon Nanotube. *Asian Journal of Chemistry* (10). vol. 25, no. 10, pp. 5467–5469. doi: 10.14233/ajchem.2013.14786.

[27] Binbin Chang, Yanzhen Guo, Yanchun Li, Hang Yin, Shouren Zhang, Baocheng Yang & Xiaoping Dong. (2015). Graphitized hierarchical porous carbon nanospheres: simultaneous activation/graphitization and superior supercapacitance performance. *Journal of Materials Chemistry A*. vol. 3, no. 18, pp. 9565–9577. doi: 10.1039/C5TA00867K.

[28] S. Goswami, P. Banerjee, S. Datta, A. Mukhopadhayay, & P. Das. (2017). Graphene oxide nanoplatelets synthesized with carbonized agro-waste biomass as green precursor and its application for the treatment of dye rich wastewater. *Process Safety and Environmental Protection*. vol. 106, pp. 163–172. doi: 10.1016/j.psep.2017.01.003.

[29] P. Aliprandini, M. M. Veiga, B. G. Marshall, T. Scarazzato & D. C. R. Espinosa. (2020). Investigation of mercury cyanide adsorption from synthetic wastewater aqueous solution on granular activated carbon. *Journal of Water Process Engineering*. vol. 34, p. 101154. doi: 10.1016/j.jwpe.2020.101154.

[30] N. Dwivedi, C. Balomajumder & P. Mondal. (2016). Comparative investigation on the removal of cyanide from aqueous solution using two different bioadsorbents. *Water Resources and Industry*. vol. 15, pp. 28–40. doi: 10.1016/j.wri.2016.06.002.

[31] N. Singh & C. Balomajumder. (2016), Simultaneous removal of phenol and cyanide from aqueous solution by adsorption onto surface modified activated carbon prepared from coconut shell. *Journal of Water Process Engineering*. vol. 9, pp. 233–245. doi: 10.1016/j.jwpe.2016.01.008.

[32] A. Behnamfard & M. M. Salarirad. (2009). Equilibrium and kinetic studies on free cyanide adsorption from aqueous solution by activated carbon. *Journal of Hazardous Materials*. vol. 170, no. 1, pp. 127–133 doi: 10.1016/j.jhazmat.2009.04.124.

[33] VJ Landin-Sandoval, DI Mendoza-Castillo, A. Bonilla-Petriciol, IA Aguayo-Villarreal, SE Reynel-Avila & HA Gonzalez-Ponce. (2020). Valorization of agri-food industry wastes to prepare adsorbents for heavy metal removal from water. Journal of Environmental Chemical Engineering. vol. 8, no. 5. doi: 10.1016/j.jece.2020.104067.

[34] Y. Zhu, B. Yi, Q. Yuan, Y. Wu, M. Wang, & S. Yan. (2018). Removal of methylene blue from aqueous solution by cattle manure-derived low temperature biochar. *RSC Advances*. vol. 8, no. 36, pp. 19917–19929. doi: 10.1039/c8ra03018a.

[35] F. Mekhalef Benhafsa, S. Kacha, A. Leboukh & K. D. Belaid. (2018). Étude comparative de l'adsorption du colorant Victoria Bleu Basique à partir de solutions aqueuses sur du carton usagé et de la sciure de bois. *Revue des sciences de l'eau*. vol. 31, no. 2, pp. 109–126. doi: 10.7202/1051695ar.

[36] S. Kundu & A. K. Gupta. (2006). Arsenic adsorption onto iron oxide-coated cement (IOCC): Regression analysis of equilibrium data with several isotherm models and their optimization. *Chemical Engineering Journal*. vol. 122, no. 1–2, pp. 93–106. doi: 10.1016/j.cej.2006.06.002.

[37] Edet, Uduakobong A & Ifelebuegu, A. O. (2020). Kinetics, Isotherms, and Thermodynamic Modeling of the Adsorption of Phosphates from Model Wastewater Using Recycled Brick Waste. *Process*. (8). doi: 10.3390/pr8060665.